Published in IET Generation, Transmission & Distribution
Received on 31st August 2010
Revised on 7th January 2011
doi: 10.1049/iet-gtd.2010.0565

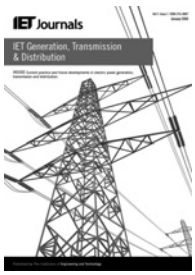

ISSN 1751-8687

Enhanced demodulation-based technique for estimating the parameters of fundamental component in power systems

C.A.G. Marques[1] *M.V. Ribeiro*[2] *E.A.B. da Silva*[1]

[1]*Federal University of Rio de Janeiro Cx. P. 68504, Rio de Janeiro, Brazil*
[2]*Federal University of Juiz de Fora, Electrical Engineering Post-Graduation Building Campus Universitário, Juiz de Fora, Brazil*
E-mail: cristiano.marques@engenharia.utjf.br

Abstract: The recent introduction of smart grid concepts in power systems demands metering and monitoring equipments with great deal of flexibility. To achieve this, one heavily depends upon new generation of signal processing tools. Regarding low-cost and effective signal processing-based techniques for parameters estimation in smart grids, the estimation of power components when frequency deviates from its nominal value is a timely and important issue to be addressed. The authors outline a demodulation-based technique for estimating the amplitude, phase and frequency of the fundamental component of a power line signal. This technique makes use of a finite impulse response filter design method that efficiently allocates zeros over the unit circle of the z-plane so that the performance losses yielded by power frequency deviations can be minimised if the signal is corrupted by harmonics. Numerical results indicate that the proposed technique outperforms previous ones and can be a good candidate for measurement and monitoring in flexible power systems.

1 Introduction

Amplitude, phase and frequency for metering and monitoring applications are very important quantities. This has been particularly true since the advent of smart grid in the last years, when their correct estimation has been receiving a great deal of attention. The smart grid can be viewed as a new paradigm that the digital revolution has brought to the existing electricity infrastructure. A smart grid is expected to be self-healing, highly fault-tolerant, efficient, reliable, secure and flexible. To have these functionalities, precise and low-cost real-time signal processing tools need to be designed. Regarding parameter estimation of power components, several signal processing techniques have been developed so far. Conventional techniques for amplitude and phase estimations, such as discrete Fourier transform (DFT) [1, 2], assume that the power line signal has constant power frequency. Consequently, DFT-based techniques can produce unreliable results when the signal suffers for frequency deviations. To estimate the power frequency, the most used techniques are based on phase-locked loops (PLLs) [3–5]. In these cases, a significant tracking delay in the estimate is observed, especially if a prefiltering stage is adopted to improve the accuracy of the estimation when the signal is polluted by harmonics.

Other techniques worth mentioning include least-squares (LS) [6, 7], the Newton method [8], the Prony method [9] and Kalman filters [10, 11]. Some of these techniques can estimate either only frequency or only amplitude and phase. A few of them can estimate all the three parameters (amplitude, phase and frequency) using only one structure. Interesting approaches are the demodulation-based techniques introduced in [12–15]. While the technique outlined in [13] is capable of estimating phase, those ones addressed in [12, 14, 15] can estimate frequency. However, amplitude estimation using demodulation-based techniques has not been explored up to date because of the difficulty in designing filters that deal properly with deviations of the power frequency. In fact, the main difficulty in designing demodulation-based techniques is the appropriate selection and design of filters to achieve the needed performance [15].

Owing to the level of flexibility needed in power systems to implement the smart grid paradigm, the investigation of estimation techniques capable of providing a small error in the estimation of fundamental amplitude and phase under frequency deviation and harmonic pollution is a timely research issue. Another important issue that must be dealt with is the increase of presence of harmonics in power systems. It makes the estimation of amplitude and phase of the fundamental component difficult when the frequencies of the harmonics are time-varying. Note that the frequency of a harmonic component suffers a deviation that increases proportionally with its order. Thus, even if a small deviation occurs in fundamental component, the deviation in the harmonics may be significant. This demands methods which are robust to large frequency deviations. Note that the DFT is a good choice for estimating the amplitude and phase of the fundamental component in the presence of harmonics when the power frequency is constant. However,

the deviation of harmonic frequencies severally degrades its estimates if power frequency deviates.

This work proposes a technique to deal with this problem: it aims at decreasing the estimation error of the parameters of a power signal for metering and monitoring applications when the power frequency and subsequent harmonic frequencies deviate from its nominal values. For this purpose we propose in this paper a design strategy for a low-pass (LP) finite impulse response (FIR) filter that improves the performance of the demodulation-based technique. We obtain improvements in two aspects: First, the estimation accuracy of the amplitude, phase and frequency of the fundamental component has been improved through proper design of a singer filter. Second, the proposed technique works well when frequency deviation of power frequency occurs and harmonics are present. Additionally, we present a general FIR filter prototype design that allows us to specify levels of estimation accuracy by taking into account the magnitude of the frequency deviation and the estimation delay.

2 Formulation of the proposed technique

Consider the monitored power line signal expressed by

$$x(t) = A_1(t)\cos[\Omega_0 t + \phi_1(t)] + \eta(t) \tag{1}$$

where $A_1(t)$ and $\phi_1(t)$ are the instantaneous fundamental amplitude and phase, respectively. Ω_0 is the synchronous fundamental angular frequency and $\eta(t)$ denotes the sum of harmonics and noise.

Now, consider the demodulation signals

$$d_c(t) = \cos(\Omega_d t) \tag{2}$$

and

$$d_s(t) = \sin(\Omega_d t) \tag{3}$$

where Ω_d refers to demodulation frequency. Multiplying $x(t)$ by $d_c(t)$ and $d_s(t)$, and assuming that $\Omega_d = \Omega_0$, one obtains

$$y_c(t) = \frac{A_1(t)}{2}\cos[\phi_1(t)] + \frac{A_1(t)}{2}\cos[2\Omega_0 t + \phi_1(t)] + \eta(t)\cos[\Omega_0 t] \tag{4}$$

and

$$y_s(t) = -\frac{A_1(t)}{2}\sin[\phi_1(t)] + \frac{A_1(t)}{2}\sin[2\Omega_0 t + \phi_1(t)] + \eta(t)\sin[\Omega_0 t] \tag{5}$$

respectively.

If one considers that $\phi_1(t)$ varies slowly, (4) and (5) imply that both $y_c(t)$ and $y_s(t)$ have a direct current (DC) component, a sinusoidal component at $2\Omega_0$ and a wideband spectral component due to the modulation of $\eta(t)$. The DC components can be extracted by applying a LP filter, yielding

$$y_{cc}(t) = \frac{A_1(t)}{2}\cos[\phi_1(t)] + \eta_c(t) \tag{6}$$

and

$$y_{ss}(t) = -\frac{A_1(t)}{2}\sin[\phi_1(t)] + \eta_s(t) \tag{7}$$

where $\eta_c(t)$ and $\eta_s(t)$ are the LP versions of $\eta(t)\cos[\Omega_0 t]$ and $\eta(t)\sin[\Omega_0 t]$.

Supposing that the LP filter is narrow enough, the components $\eta_c(t)$ and $\eta_s(t)$ can be considered negligible, and then the amplitude and phase of the target signal can be estimated by

$$\hat{A}_1(t) = 2\sqrt{y_{cc}(t)^2 + y_{ss}(t)^2} \tag{8}$$

and

$$\hat{\phi}_1(t) = -\arctan\left(\frac{y_{ss}(t)}{y_{cc}(t)}\right) \tag{9}$$

respectively.

Additionally, the frequency can be estimated from the definition of the instantaneous frequency deviation [12], which is expressed by

$$\Delta f_i(t) = \frac{1}{2\pi}\frac{d\phi_1(t)}{dt} \tag{10}$$

Thus, the estimated instantaneous frequency can be expressed by

$$\hat{f}_1(t) = f_0 + \Delta f_i(t) = f_0 + \frac{1}{2\pi}\frac{d\hat{\phi}_1(t)}{dt} \tag{11}$$

where $f_0 = \Omega_0/(2\pi)$ is the synchronous frequency.

Note that the development of the above equations considers $\Omega_0 = \Omega_d$. For the case of $\Omega_0 \neq \Omega_d$, $y_{cc}(t)$ and $y_{ss}(t)$ are given by

$$y_{cc}(t) = \frac{A_1(t)}{2}\cos[(\Omega_0 - \Omega_d)t + \phi_1(t)] + \eta_c(t) \tag{12}$$

and

$$y_{ss}(t) = -\frac{A_1(t)}{2}\sin[(\Omega_0 - \Omega_d)t + \phi_1(t)] + \eta_s(t) \tag{13}$$

respectively.

Equations (8)–(11) still apply. Details can be found in Appendix Section 7.1.

Based on this formulation, the block diagram of the proposed technique is illustrated in Fig. 1. The LP blocks implement equal LP filters and the blocks COS and SIN implement the demodulations signals expressed by (2) and (3), respectively. Details of the blocks AMP, PHAS and FREQ are shown in Fig. 2. In this figure, the blocks SQRT,

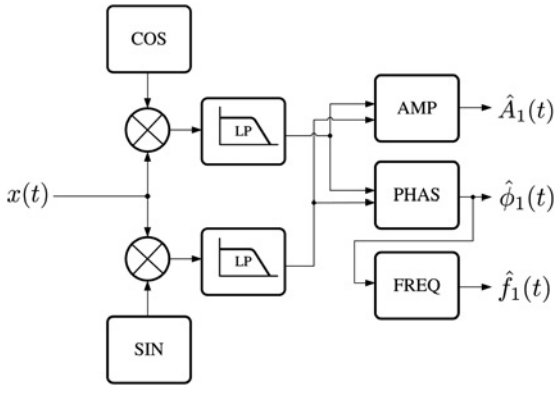

Fig. 1 *Block diagram of the proposed technique*

doi: 10.1049/iet-gtd.2010.0565

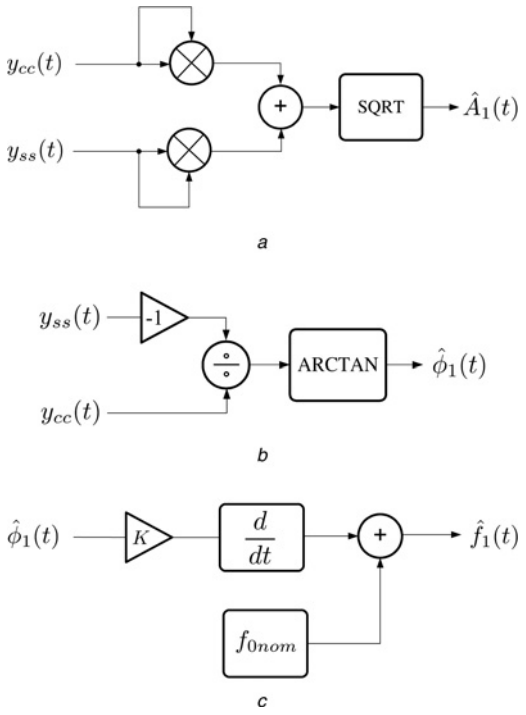

Fig. 2 *Details of the blocks*

a AMP
b PHAS
c FREQ

ARCTAN, K, $f_{0\,\mathrm{nom}}$ represent the square root, arctangent, $(1/2\pi)$ gain and nominal synchronous frequency, respectively.

3 Implementation of the proposed technique

This section presents the implementation of a discrete version of the proposed technique. With it we aim to obtain accuracy under the presence of harmonic components and frequency deviations.

The discrete version of the signal in (1) is given by

$$x[n] = A_1[n]\cos(w_0 n + \phi_1[n]) + \eta[n] \tag{14}$$

where f_s is the sampling rate and $w_0 = (\Omega_0/f_s)$ is the digital synchronous angular frequency.

The demodulation signals in (2) and (3) become

$$d_c[n] = \cos(w_d n) \tag{15}$$

and

$$d_s[n] = \sin(w_d n) \tag{16}$$

respectively, where $w_d = \Omega_d/f_s$ is the digital demodulation frequency. We consider $w_d = w_{0\,\mathrm{nom}}$, where $w_{0\,\mathrm{nom}}$ is the nominal value of w_0. Note that, as the frequency w_d is constant, then one-cycle of the demodulation signals (2) and (3) can be stored for hardware implementation.

In what follows, we will consider that the predominant distortion in signal $x[n]$ is the presence of harmonics, that is

$$\begin{aligned} x[n] = {} & A_1[n]\cos(w_0 n + \phi_1[n]) + A_2[n]\cos(2w_0 n + \phi_2[n]) \\ & + A_3[n]\cos(3w_0 n + \phi_3[n]) + A_4[n]\cos(4w_0 n + \phi_4[n]) \\ & + \cdots + A_m[n]\cos(mw_0 n + \phi_m[n]) + \cdots \end{aligned} \tag{17}$$

If the angular frequency w_0 varies from $w_{0a} = w_{0\,\mathrm{nom}} - \Delta w_0$ to $w_{0b} = w_{0\,\mathrm{nom}} + \Delta w_0$, the spectrum of the demodulated signal varies in the frequency ranges $[0 \quad w_{0\,\mathrm{nom}} - w_{0a}]$, $[2w_{0a} - w_{0\,\mathrm{nom}} \quad 2w_{0b} - w_{0\,\mathrm{nom}}]$, $[3w_{0a} - w_{0\,\mathrm{nom}} \quad 3w_{0b} - w_{0\,\mathrm{nom}}]$, …, $[(m+1)w_{0a} - w_{0\,\mathrm{nom}} \quad (m+1)w_{0b} - w_{0\,\mathrm{nom}}]$…. Fig. 3 depicts these ranges and the center frequencies $w_{0\,\mathrm{nom}}$, $2w_{0\,\mathrm{nom}}$, $3w_{0\,\mathrm{nom}}$, …, $mw_{0\,\mathrm{nom}}$, …. Each os these ranges (except the range around 0 Hz) is defined by

$$\Delta w_m = (m+1)(w_{0b} - w_{0a}) \tag{18}$$

where $m = 1, 2, 3, \ldots$. See Appendix Section 7.2 for the derivation of these ranges.

The LP filtering of the demodulated signal can be implemented either with a standard infinite impulse response (IIR) or FIR LP filter. IIR filters offer good attenuation at the stop-band and have few coefficients compared with FIR filters; however, they exhibit longer transient response and difficulties for hardware implementation due to stability concerns. Moreover, they do not have linear-phase, which may be a source of error in phase estimation.

If there is no deviation in the nominal frequency, a simple solution is the use of the moving-average filter [16]. This filter rejects all harmonics components of the demodulated signal if the signal frequency is constant and equals to nominal value (Fig. 4*a*). However, if the frequency suffers a slight change (see example in Fig. 4*b*), the zeros of the filter do not match the locations of the harmonics of the demodulated signal. As a result, such filtering will offer poor estimation.

To correctly remove harmonic components from demodulated signal and provide low estimation delay, a suitable choice is an FIR LP filter with a good attenuation in the frequency bands as shown in Fig. 3. We have designed such a filter using the weighted-least-squares (WLS) method [17].

In short, filter's specifications on the WLS algorithm are depicted in Fig. 5, where δ_p is the ripple of the passband and $1 - \delta_s$ is the attenuation in the neighbourhood of the harmonics. In this paper, the design of the filter was based on the following constraints: an attenuation larger than 90 dB was expected in the neighbourhood of the harmonics and a ripple of 3×10^{-5} dB was expected in the passband. The filter order was increased heuristically in the WLS algorithm until the frequency response achieved the required specifications. A 97th-order LP filter was obtained

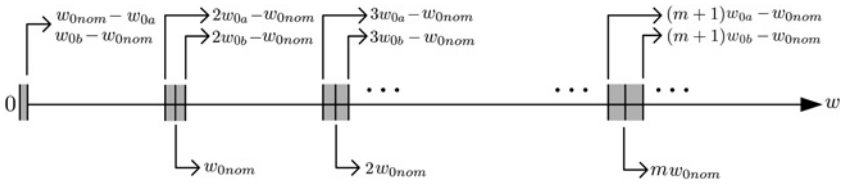

Fig. 3 *Spectrum location of the demodulated signal when harmonics are present and power frequency varies from w_{0a} to w_{0b}*

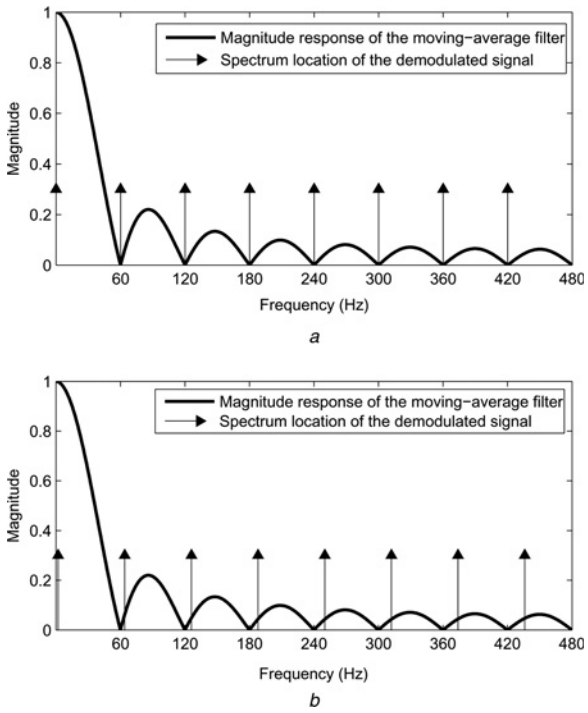

Fig. 4 *Magnitude response of the moving-average filter and the spectrum locations of the demodulation signal*

a When the frequency is constant and equals to nominal value
b When the frequency suffer a slight change

and its magnitude response is shown in Fig. 6. The magnitude response of the moving-average filter is also shown in the same figure for comparison purposes. Fig. 7 shows a zoom of the magnitude response around 180 Hz. The length of the designed filter corresponds to three cycles of the fundamental component, which also corresponds to the time delay of the estimation, and thus determines the speed of convergence of the algorithm.

In the WLS algorithm, the frequency axis was divided into N sets of frequency bands, and the frequency bands incident in the frequency ranges shown in Fig. 3 were weighted for optimisation. Note that the passband must include the range $[0 w_{0b} - w_{0\text{nom}}]$. For getting the numerical results shown in Figs. 6 and 7 (that are used in the subsequent section), the following parameters were taken into account: $N = 3840$, $w_c = 2\pi 2/f_s$, $w_{0\text{nom}} = 2\pi 60/f_s$, $\Delta w_0 = 2\pi 0.5/f_s$, and $f_s = 32 \times 60$ Hz. The weights for the frequencies less than or equal to w_c are equal to 1000; for the other bands around $mw_{0\,\text{nom}}$ (see Fig. 3) they are equal to 20. These values have been determined experimentally to achieve the needed specifications. The variation $\Delta w_0 = 2\pi 0.5/f_s$ corresponding to the variation $\Delta f_0 = 0.5$ Hz is sufficient for most power system applications. This is so because frequency variations are usually smaller than ± 0.1 Hz [18] in interconnected grids. Note that this variation is a design parameter and can be adapted to more or less demanding cases. For example, in isolated systems such as shipboard power systems this variation can achieve ± 3 Hz in 60 Hz systems [19].

The amplitude, phase and frequency evaluations are carried out sample-by-sample. The discrete version of the frequency

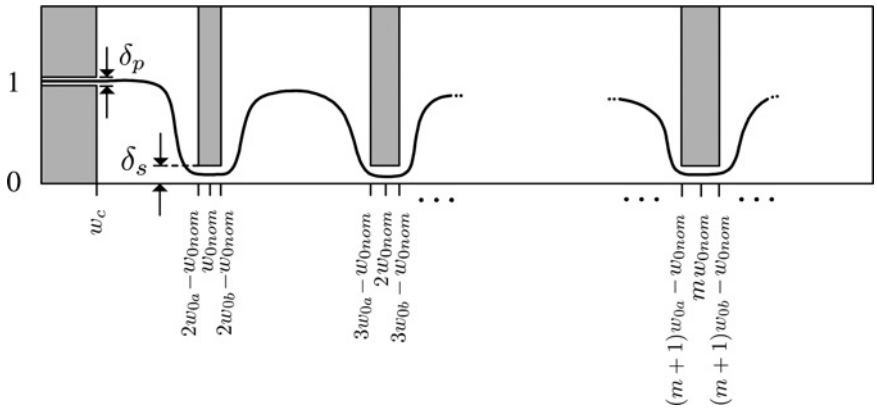

Fig. 5 *Filter's specifications*

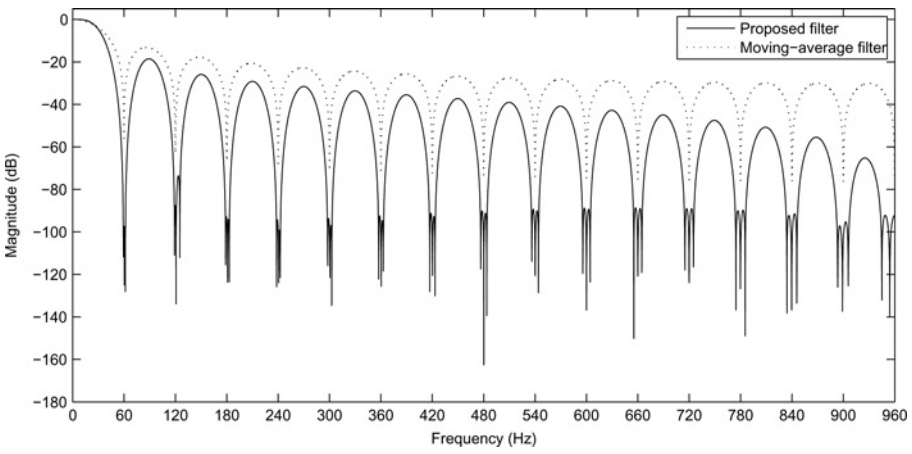

Fig. 6 *Magnitude response of the designed filter*

doi: 10.1049/iet-gtd.2010.0565

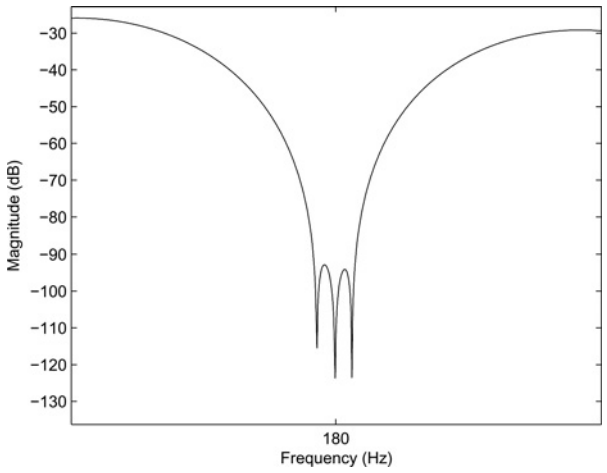

Fig. 7 *Zoom at 180 Hz in the magnitude response of the designed filter*

estimator in (11) is given by

$$\hat{f}_1[n] = f_0 + \frac{f_s}{2\pi}(\hat{\phi}_1[n] - \hat{\phi}_1[n-1]) \tag{19}$$

4 Performance analysis

In this section a performance analysis of the proposed technique is presented. For all simulations, the sampling rate is equal to $f_s = 32 \times 60$ Hz and the LP filter used is the same one described in Section 3, (magnitude response shown in Fig. 6).

4.1 Tracking performance

Tracking performances of the proposed technique are presented in Fig. 8 for amplitude, phase and frequency estimations. For evaluating the performance of amplitude estimation, we introduce to a sinusoidal signal a momentary interruption. For evaluating the performance of phase estimation, the sinusoidal signal undergoes a phase jump from $\pi/4$ to $-\pi/4$ rad. And, for evaluating the performance of frequency estimation, we introduce a change in frequency from 60 to 59.5 Hz. The delay of the estimation is about three cycles of the fundamental component for all cases.

4.2 Error performance

For error performance analysis, the generated signal is given by

$$\begin{aligned} x[n] = {} & \cos(w_0 n) + \frac{1}{3}\cos(3w_0 n) + \frac{1}{5}\cos(5w_0 n) \\ & + \frac{1}{7}\cos(7w_0 n) + \frac{1}{9}\cos(9w_0 n) + \frac{1}{11}\cos(11w_0 n) \\ & + \frac{1}{13}\cos(13w_0 n) + \frac{1}{15}\cos(15w_0 n) + v[n] \end{aligned} \tag{20}$$

where $v[n]$ is a zero-mean white Gaussian noise so that the signal-to-noise ratio (SNR) is 60 dB. It should be noted that the SNR of the signal obtained from a power system usually ranges between 50 and 70 dB [20]. Then, several signals given by (20) were generated by varying the fundamental frequency from 59.5 to 60.5 Hz. The evaluation of the error is based on the calculation of the maximum of the absolute instantaneous

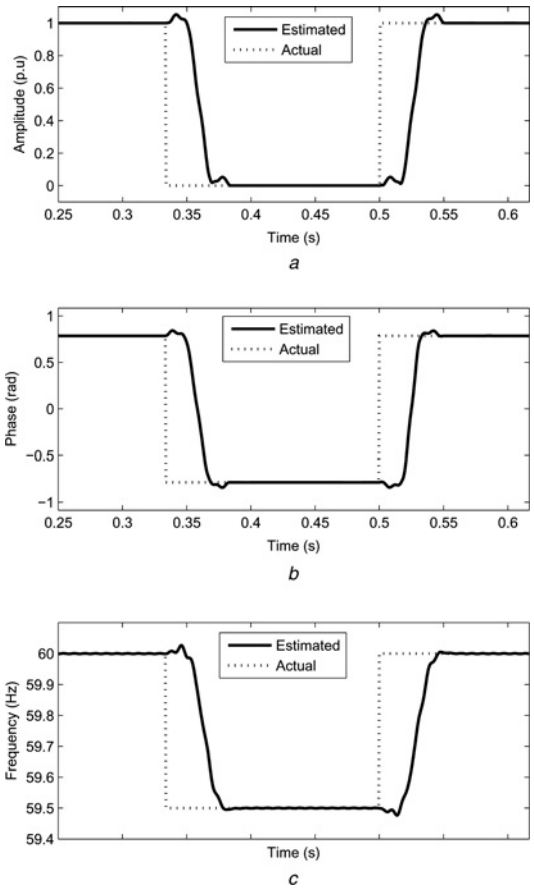

Fig. 8 *Tracking performances*

a Amplitude tracking performance when a momentary interruption occurs
b Phase tracking performance when a phase jump from $\pi/4$ to $-\pi/4$ rad occurs in the signal
c Frequency tracking performance when the frequency changes from 60 to 59.5 Hz

error of the estimate. The results are presented in Fig. 9. Note that the error is lower than 0.05%, 0.1% and 0.8% for amplitude, phase and frequency estimation, respectively.

4.3 Performance comparison to conventional techniques

In this section, we present a comparative performance evaluation of the proposed technique with two conventional methods: DFT [1] and EPLL [5].

Figs. 10–12 illustrate the tracking performance of all techniques when a failure takes place in a hypothetic power system considering the following signal

$$\begin{aligned} x[n] = {} & \cos(w_0 n + \phi_1[n]) + \frac{1}{3}\cos(3w_0 n + \phi_3[n]) \\ & + \frac{1}{5}\cos(5w_0 n + \phi_5[n]) + \frac{1}{7}\cos(7w_0 n + \phi_7[n]) \\ & + \frac{1}{9}\cos(9w_0 n + \phi_9[n]) + \frac{1}{11}\cos(11w_0 n + \phi_{11}[n]) \\ & + \frac{1}{13}\cos(13w_0 n + \phi_{13}[n]) \\ & + \frac{1}{15}\cos(15w_0 n + \phi_{15}[n]) + v[n] \end{aligned} \tag{21}$$

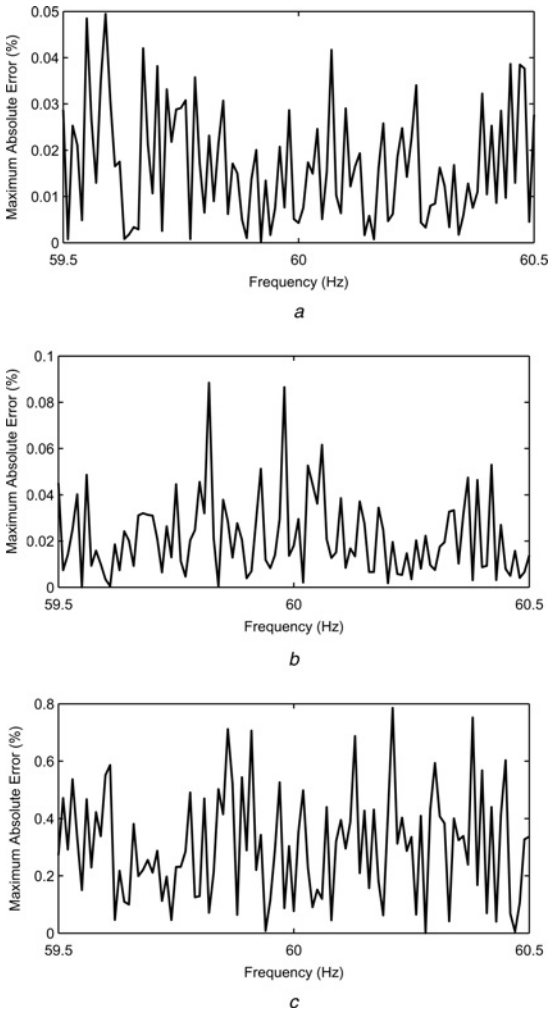

Fig. 9 *Maximum absolute error*

a Amplitude estimation
b Phase estimation
c Frequency estimation when the frequency of the signal given by (20) varies from 59.5 to 60.5 Hz

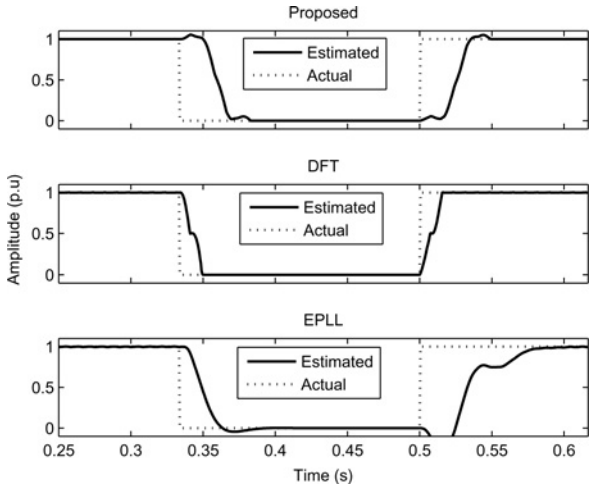

Fig. 10 *Comparison of tracking performance for amplitude estimation*

where $\phi_1[n] = \pi/4$, $\phi_3[n] = \phi_5[n] = \phi_7[n] = \phi_9[n] = \phi_{11}[n] = \phi_{13}[n] = \phi_{15}[n] = 0$ and $v[n]$ is a zero-mean white Gaussian noise so that the SNR is 60 dB. For evaluating the performance of amplitude estimation, we introduce to the signal a momentary interruption assuming $f_0 = 60.1$ Hz. For evaluating the performance of phase estimation, the fundamental component undergoes a phase jump from $\phi_1[n] = \pi/4$ to $\phi_1[n] = -\pi/4$ rad assuming $f_0 = 60.1$ Hz. And, for evaluating the performance of frequency estimation, we introduce a change in frequency from $f_0 = 60$ Hz to $f_0 = 59.9$ Hz. Note that in Fig. 12, the DFT method has not been included because the DFT is unable to estimate frequency deviations.

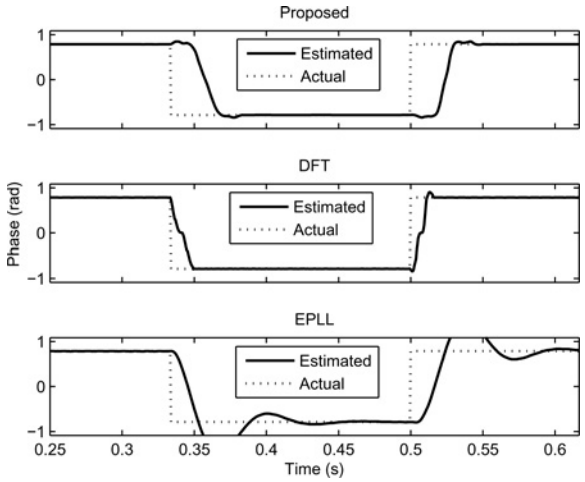

Fig. 11 *Comparison of tracking performance for phase estimation*

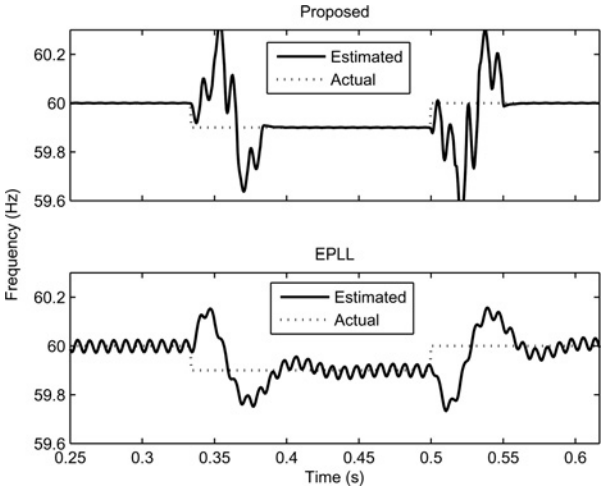

Fig. 12 *Comparison of tracking performance for frequency estimation*

In order to show more clearly the error in the time estimations, Fig. 13 illustrates a zoom in the time-estimates of amplitude of the signal (37) with the three techniques. It is noted that the estimates using the DFT and EPLL algorithms provide larger variations.

For the signal given in (20), the attained maximum absolute instantaneous errors are shown in Figs. 14–16. The results shown indicate that the EPLL exhibits longer delay than other techniques, that is, about 5 cycles. Regarding the DFT technique, it offers fast tracking, of about 1 cycle, and very good error performance when $f_0 = 60$ Hz, however, if the deviation from $f_0 = 60$ Hz increases, then its performance drops considerably. On the other hand, the proposed demodulation-based technique offers satisfactory results.

doi: 10.1049/iet-gtd.2010.0565

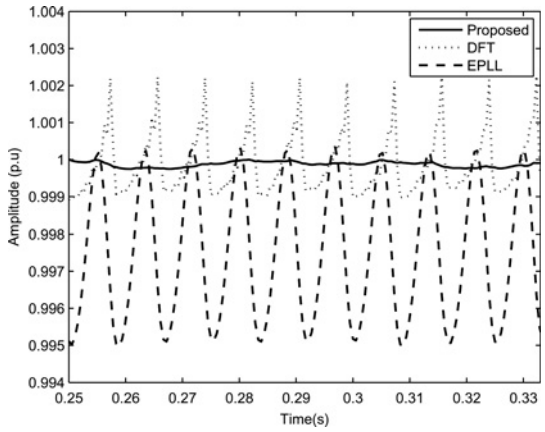

Fig. 13 *Zoom in the amplitude estimates with the proposed, DFT and EPLL techniques*

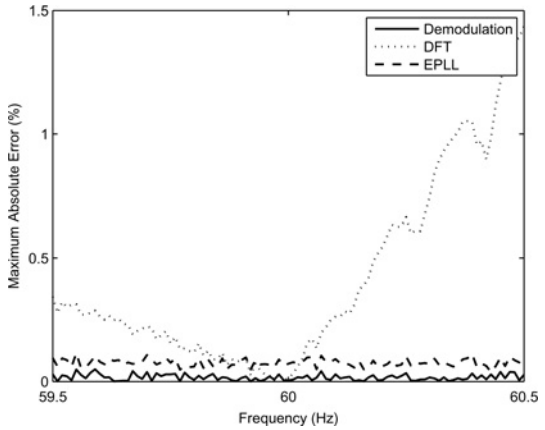

Fig. 14 *Maximum absolute error comparison of amplitude estimation when the frequency of the signal given by (20) varies from 59.5 to 60.5 Hz*

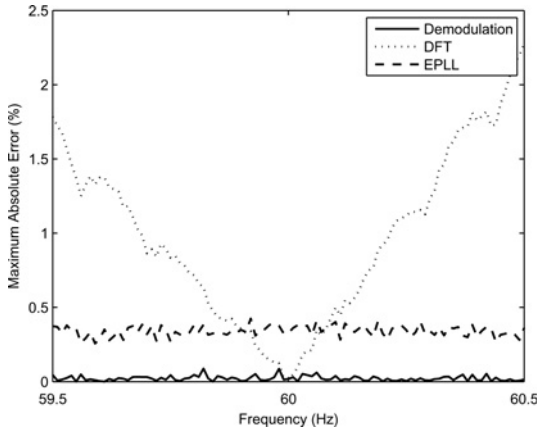

Fig. 15 *Maximum absolute error comparison of phase estimation when the frequency of the signal given by (20) varies from 59.5 to 60.5 Hz*

One has to note that the results of the proposed technique presented so far were attained by using the 97th-order FIR filter discussed in Section 3. However, the filter order can be increased for offering more accuracy, or decreased for shortening the estimation delay. In Fig. 17 it is shown a magnitude response for a filter design considering

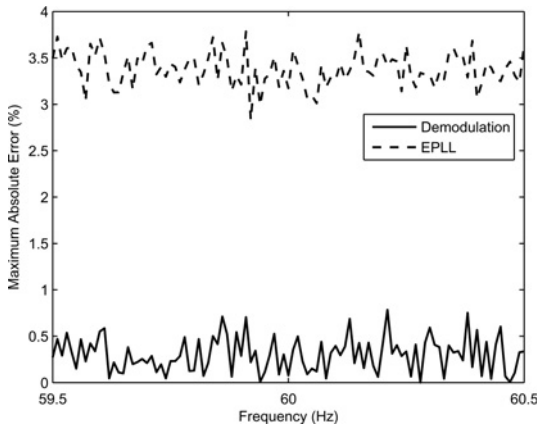

Fig. 16 *Maximum absolute error comparison of frequency estimation when the frequency of the signal given by (20) varies from 59.5 to 60.5 Hz*

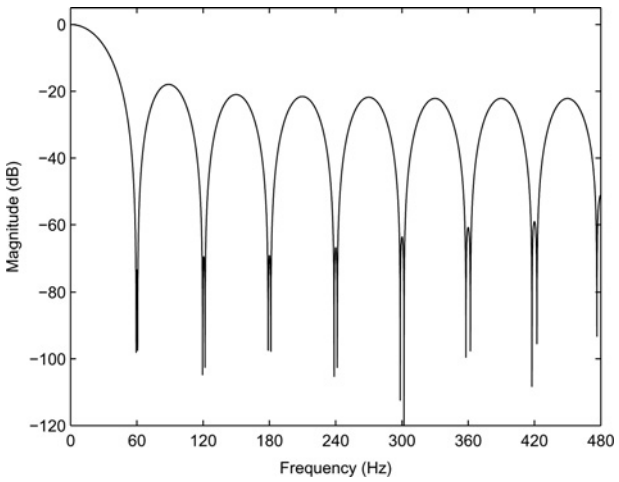

Fig. 17 *Magnitude response of the proposed filter design considering $f_s = 16 \times 60$ Hz and delay of two cycles of the fundamental component*

$f_s = 16 \times 60$ Hz, which achieves a delay of two cycles of the fundamental component. In this design a 33th-order FIR filter was achieved. As a result, the estimation delay is shortened at the cost of a decrease in accuracy. However, in applications such as measurement, the accuracy of the results is more important than speed; therefore, a filter with higher order can be designed.

5 Concluding remarks

In this contribution we have addressed the suitability of demodulation-based techniques for estimating amplitude, phase and frequency of the fundamental component under power frequency variation scenarios. This kind of technique is especially attractive for smart or micro-grid applications. The main improvement regarding it is the suggestion of new FIR filter design procedure, which can offer an improved performance under the presence of harmonics and frequency deviations.

Although the filter has been designed taking into account a frequency deviation lower than 0.5 Hz around the nominal power frequency, the filter's design specifications can be

modified to cope with larger deviations while maintaining the same estimation error performance. This can be achieved at the expenses of an increase in the filter length, and, consequently in the estimation delay. Therefore there is a compromise between performance, flexibility and delay estimation that must be considered a priori.

Comparison results have pointed towards the attractiveness of the proposed demodulation-based technique for power system applications under the presence of power frequency deviations, harmonics and noise. Furthermore, this technique can have an appealing role in the development of low-cost monitoring devices for smart-grid applications due to the reduced computational burden associated with it.

6 References

1 Phadke, A.G., Thorp, J.S.: 'Computer relaying for power systems' (Wiley, 1988)
2 Thorp, J.S., Phadke, A.G., Karimi, K.J.: 'Real-time voltage phasor measurements for static-state estimation', *IEEE Trans. Power Appl. Syst.*, 1985, **11**, (PAS 11), pp. 3099–3106
3 Carvalho, J.R., de Duque, C.A., Ribeiro, M.V., Cerqueira, A.S., Baldwin, T.L., Ribeiro, P.F.: 'A PLL-based multirate structure for time-varying power systems harmonic/interharmonic estimation', *IEEE Trans. Power Deliv.*, 2009, **24**, (4), pp. 1789–1800
4 Gomes, P.C., Ribeiro, M.V., Duque, C.A., Cerqueira, A.S.: 'Enhanced and robust phase-locked-loop structure for parameters estimation of power line signals'. Int. Conf. Harmonics and Power Quality, Cascais, Portugal, 2007
5 Ghartemani, M.K., Iravani, M.R.: 'Robust and frequency-adaptive measurement of peak value', *IEEE Trans. Power Deliv.*, 2004, **19**, (2), pp. 481–489
6 Chudamani, R., Vasudevan, K., Ramalingam, C.S.: 'Real-time estimation of power system frequency using nonlinear least squares', *IEEE Trans. Power Deliv.*, 2009, **24**, (3), pp. 1021–1028
7 Sachdev, M.S., Giray, M.M.: 'A least error squares technique for determining power system frequency', *IEEE Trans. Power Appar. Syst.*, 1985, **PAS-104**, (2), pp. 437–443
8 Terzija, V.V., Djuric, M.B., Kovacevic, B.D.: 'Voltage phasor and local system frequency estimation using Newton type algorithm', *IEEE Trans. Power Deliv.*, 1994, **9**, (3), pp. 1368–1374
9 Lobos, T., Rezmer, R.J.: 'Real-time determination of power system frequency', *IEEE Trans. Instrum. Meas.*, 1997, **46**, (4), pp. 877–881
10 Dash, P.K., Jena, R.K., Panda, G., Routray, A.: 'An extended complex Kalman filter for frequency measurement of distorted signals', *IEEE Trans. Instrum. Meas.*, 2000, **49**, (4), pp. 746–753
11 Routray, A., Pradhan, A.K., Rao, K.P.: 'A novel Kalman filter for frequency estimation of distorted signals in power systems', *IEEE Trans. Instrum. Meas.*, 2002, **51**, (3), pp. 469–479
12 Begović, M.M., Djurić, P.M., Dunlap, S., Phadke, A.G.: 'Frequency tracking in power networks in the presence of harmonics', *IEEE Trans. Power Deliv.*, 1993, **8**, (2), pp. 480–486
13 Djurić, P.M., Begović, M.M., Doroslovaki, M.: 'Instantaneous phase tracking in power networks by demodulation', *IEEE Trans. Instrum. Meas.*, 1992, **41**, (6), pp. 963–967
14 Akke, M.: 'Frequency estimation by demodulation of two complex signals', *IEEE Trans. Power Deliv.*, 1997, **12**, (1), pp. 157–163
15 Kamwa, I., Leclerc, M., McNabb, D.: 'Performance of demodulation-based frequency measurement algorithms used in typical PMUs', *IEEE Trans. Power Deliv.*, 2004, **19**, (2), pp. 505–514
16 Oppenheim, A.V., Schafer, R.W., Buck, J.R.: 'Discrete-time signal processing' (Prentice-Hall, 1999, 2nd edn.)
17 Diniz, P.S.R., da Silva, E.A.B., Netto, S.L.: 'Digital signal processing: system analysis and design' (Cambridge University Press, 2002)
18 IEEE Std 1531–2003: 'IEEE guide for application and specification of harmonic filters', 2003
19 IEEE Std 1662–2008: 'IEEE guide for the design and application of power electronics in electrical power systems on ships', 2008
20 Tomić, J.J., Kušljevic, M.D., Vujicić, V.V.: 'A new power system digital harmonic analyzer', *IEEE Trans. Power Deliv.*, 2007, **22**, (2), pp. 772–780

7 Appendix

7.1 Parameters estimation when $\Omega_0 \cong \Omega_d$

Consider the monitored power line signal given by (1) and the demodulation signals expressed by (2) and (3).

Multiplying $x(t)$ by $d_c(t)$ and $d_s(t)$, one obtains

$$y_c(t) = \frac{A_1(t)}{2}\cos[(\Omega_0 - \Omega_d)t + \phi_1(t)] + \frac{A_1(t)}{2}\cos[(\Omega_0 + \Omega_d)t + \phi_1(t)] + \eta(t)\cos[\Omega_0 t] \tag{22}$$

and

$$y_s(t) = -\frac{A_1(t)}{2}\sin[(\Omega_0 - \Omega_d)t + \phi_1(t)] + \frac{A_1(t)}{2}\sin[(\Omega_0 + \Omega_d)t + \phi_1(t)] + \eta(t)\sin[\Omega_0 t] \tag{23}$$

respectively.

Considering that $\phi_1(t)$ varies slowly, and filtering (22) and (23) by a LP filter, we have

$$y_{cc}(t) = \frac{A_1}{2}\cos[(\Omega_0 - \Omega_d)t + \phi_1(t)] + \eta_c(t) \tag{24}$$

and

$$y_{ss}(t) = -\frac{A_1}{2}\sin[(\Omega_0 - \Omega_d)t + \phi_1(t)] + \eta_s(t) \tag{25}$$

respectively, where $\eta_c(t)$ and $\eta_s(t)$ are the output of the filtered components $\eta(t)\cos[\Omega_0 t]$ and $\eta(t)\sin[\Omega_0 t]$ around DC.

Neglecting the components $\eta_c(t)$ and $\eta_s(t)$, one obtains

$$\sqrt{y_{cc}(t)^2 + y_{ss}(t)^2} = \frac{A_1(t)}{2} \tag{26}$$

and

$$\frac{y_{ss(t)}}{y_{cc(t)}} = -\tan[(\Omega_0 - \Omega_d)t + \phi_1(t)] \tag{27}$$

Thus, the amplitude can be estimated by using

$$\hat{A}_1(t) = 2\sqrt{y_{cc}(t)^2 + y_{ss}(t)^2} \tag{28}$$

For phase estimation, one has that

$$[\Omega_0 - \Omega_d]t + \phi_1(t) = -\arctan\left[\frac{y_{ss}(t)}{y_{cc}(t)}\right] \tag{29}$$

Therefore

$$\phi_1(t) = -\arctan\left[\frac{y_{ss}(t)}{y_{cc}(t)}\right] - [\Omega_0 - \Omega_d]\,t \tag{30}$$

doi: 10.1049/iet-gtd.2010.0565

Note that

$$\lim_{t\to\pm\infty}|\phi_1(t)| = \infty. \tag{31}$$

However, evaluating the phase difference of two signals $x_a(t) = A_{1a}(t)\cos[\Omega_0 t + \phi_{1a}(t)]$ and $x_b(t) = A_{1b}(t)\cos[\Omega_0 t + \phi_{1b}(t)]$ of the same power system, one obtains

$$\phi_{1a}(t) - \phi_{1b}(t) = -\arctan\left[\frac{y_{ssa}(t)}{y_{cca}(t)}\right] - [\Omega_0 - \Omega_d]t - \left[-\arctan\left[\frac{y_{ssb}(t)}{y_{ccb}(t)}\right] - [\Omega_0 - \Omega_d]t\right] \tag{32}$$

or

$$\phi_{1a}(t) - \phi_{1b}(t) = -\arctan\left[\frac{y_{ssa}(t)}{y_{cca}(t)}\right] + \arctan\left[\frac{y_{ssb}(t)}{y_{ccb}(t)}\right], \tag{33}$$

which is independent of $[\Omega_0 - \Omega_d]t$.

Thus, the phase of each signal can be estimated by

$$\hat{\phi}_1(t) = -\arctan\left[\frac{y_{ss}(t)}{y_{cc}(t)}\right]. \tag{34}$$

7.2 Spectral analysis of the demodulated power signal when only harmonics are present

Consider the power system signal corrupted only by harmonics

$$\begin{aligned} x(t) = {} & A_1(t)\cos[\Omega_0 t + \phi_1(t))] + A_2(t)\cos[2\Omega_0 t + \phi_2(t)] \\ & + A_3(t)\cos[3\Omega_0 t + \phi_3(t)] + A_4(t)\cos[4\Omega_0 t + \phi_4(t)] \\ & + \cdots + A_m(t)\cos[m\Omega_0 t + \phi_m(t)] \\ & + \cdots + A_{N_h}(t)\cos[N_h\Omega_0 t + \phi_{N_h}(t)], \end{aligned} \tag{35}$$

where $\Omega_0 = 2\pi f_0$. If the frequency Ω_0 decreases to $\Omega_{0a} = \Omega_{0\text{nom}} - \Delta\Omega_0$, where $\Omega_{0\text{nom}}$ is the nominal value of Ω_0 and $\Delta\Omega_0$ is the absolute variation of Ω_0, then the signal $x(t)$ becomes

$$\begin{aligned} x_a(t) = {} & A_1(t)\cos(\Omega_{0a}t + \phi_{1a}(t)) + A_2(t)\cos[2\Omega_{0a}t + \phi_{2a}(t)] \\ & + A_3(t)\cos[3\Omega_{0a}t + \phi_{3a}(t)] + A_4(t)\cos[4\Omega_{0a}t + \phi_{4a}(t)] \\ & + \cdots + A_m(t)\cos[m\Omega_{0a}t + \phi_{ma}(t)] \\ & + \cdots + A_{N_h}(t)\cos[N_h\Omega_{0a}t + \phi_{N_h a}(t)]. \end{aligned} \tag{36}$$

Similarly, for the increase of the frequency to $\Omega_{0b} = \Omega_{0\text{nom}} + \Delta\Omega_0$, one obtains

$$\begin{aligned} x_b(t) = {} & A_1(t)\cos[\Omega_{0b}t + \phi_{1b}(t)] + A_2(t)\cos[2\Omega_{0b}t + \phi_{2b}(t)] \\ & + A_3(t)\cos[3\Omega_{0b}t + \phi_{3b}(t)] \\ & + A_4(t)\cos[4\Omega_{0b}t + \phi_{4b}(t)] \\ & + \cdots + A_m(t)\cos[m\Omega_{0b}t + \phi_{mb}(t)] \\ & + \cdots + A_{N_h}(t)\cos[N_h\Omega_{0b}t + \phi_{N_h b}(t)]. \end{aligned} \tag{37}$$

Multiplying $x_a(t)$ by $\cos(\Omega_d t)$ and $\sin(\Omega_d t)$, where $\Omega_d = \Omega_{0\text{nom}}$, after some trigonometric manipulations one has

$$\begin{aligned} y_{ca}(t) = {} & \frac{A_1(t)}{2}\cos[(\Omega_{0a} + \Omega_{0\text{nom}})t + \phi_{1a}(t)] \\ & + \frac{A_2(t)}{2}\cos[(2\Omega_{0a} + \Omega_{0\text{nom}})t + \phi_{2a}(t)] \\ & + \frac{A_3(t)}{2}\cos[(3\Omega_{0a} + \Omega_{0\text{nom}})t + \phi_{3a}(t)] \\ & + \cdots + \frac{A_m(t)}{2}\cos[(m\Omega_{0a} + \Omega_{0\text{nom}})t + \phi_{ma}(t)] \\ & + \cdots + \frac{A_{N_h}(t)}{2}\cos[(N_h\Omega_{0a} + \Omega_{0\text{nom}})t + \phi_{N_h a}(t)] \\ & + \frac{A_1(t)}{2}\cos[(\Omega_{0a} - \Omega_{0\text{nom}})t + \phi_{1a}(t)] \\ & + \frac{A_2(t)}{2}\cos[(2\Omega_{0a} - \Omega_{0\text{nom}})t + \phi_{2a}(t)] \\ & + \frac{A_3(t)}{2}\cos[(3\Omega_{0a} - \Omega_{0\text{nom}})t + \phi_{3a}(t)] \\ & + \cdots + \frac{A_m(t)}{2}\cos[(m\Omega_{0a} - \Omega_{0\text{nom}})t + \phi_{ma}(t)] \\ & + \cdots + \frac{A_{N_h}(t)}{2}\cos[(N_h\Omega_{0a} - \Omega_{0\text{nom}})t + \phi_{N_h a}(t)] \end{aligned} \tag{38}$$

and

$$\begin{aligned} y_{sa}(t) = {} & \frac{A_1(t)}{2}\sin[(\Omega_{0a} + \Omega_{0\text{nom}})t + \phi_{1a}(t)] \\ & + \frac{A_2(t)}{2}\sin[(2\Omega_{0a} + \Omega_{0\text{nom}})t + \phi_{2a}(t)] \\ & + \frac{A_3(t)}{2}\sin[(3\Omega_{0a} + \Omega_{0\text{nom}})t + \phi_{3a}(t)] \\ & + \cdots + \frac{A_m}{2}\sin[(m\Omega_{0a} + \Omega_{0\text{nom}})t + \phi_{ma}(t)] \\ & + \cdots + \frac{A_{N_h}}{2}\sin[(N_h\Omega_{0a} + \Omega_{0\text{nom}})t + \phi_{N_h a}(t)] \\ & - \frac{A_1(t)}{2}\sin[(\Omega_{0a} - \Omega_{0\text{nom}})t + \phi_{1a}(t)] \\ & - \frac{A_2(t)}{2}\sin[(2\Omega_{0a} - \Omega_{0\text{nom}})t + \phi_{2a}(t)] \\ & - \frac{A_3(t)}{2}\sin[(3\Omega_{0a} - \Omega_{0\text{nom}})t + \phi_{3a}(t)] \\ & + \cdots - \frac{A_m(t)}{2}\sin[(m\Omega_{0a} - \Omega_{0\text{nom}})t + \phi_{ma}(t)] \\ & + \cdots - \frac{A_{N_h}}{2}\sin[(N_h\Omega_{0a} - \Omega_{0\text{nom}})t + \phi_{N_h a}(t)], \end{aligned} \tag{39}$$

respectively.

In a similar manner for the signal $x_b(t)$, one obtains

$$\begin{aligned}
y_{cb}(t) = {} & \frac{A_1(t)}{2}\cos[(\Omega_{0b} + \Omega_{0\text{nom}})t + \phi_{1b}(t)] \\
& + \frac{A_2(t)}{2}\cos[(2\Omega_{0b} + \Omega_{0\text{nom}})t + \phi_{2b}(t)] \\
& + \frac{A_3(t)}{2}\cos[(3\Omega_{0b} + \Omega_{0\text{nom}})t + \phi_{3b}(t)] \\
& + \cdots + \frac{A_m(t)}{2}\cos[(m\Omega_{0b} + \Omega_{0\text{nom}})t + \phi_{mb}(t)] \\
& + \cdots + \frac{A_{N_h}(t)}{2}\cos[(N_h\Omega_{0b} + \Omega_{0\text{nom}})t + \phi_{N_hb}(t)] \\
& + \frac{A_1(t)}{2}\cos[(\Omega_{0b} - \Omega_{0\text{nom}})t + \phi_{1b}(t)] \\
& + \frac{A_2(t)}{2}\cos[(2\Omega_{0b} - \Omega_{0\text{nom}})t + \phi_{2b}(t)] \\
& + \frac{A_3(t)}{2}\cos[(3\Omega_{0b} - \Omega_{0\text{nom}})t + \phi_{3b}(t)] \\
& + \cdots + \frac{A_m(t)}{2}\cos[(m\Omega_{0b} - \Omega_{0\text{nom}})t + \phi_{mb}(t)] \\
& + \cdots + \frac{A_{N_h}(t)}{2}\cos[(N_h\Omega_{0b} - \Omega_{0\text{nom}})t + \phi_{N_hb}(t)]
\end{aligned} \tag{40}$$

and

$$\begin{aligned}
y_{sb}(t) = {} & \frac{A_1(t)}{2}\sin[(\Omega_{0b} + \Omega_{0\text{nom}})t + \phi_{1b}(t)] \\
& + \frac{A_2(t)}{2}\sin[(2\Omega_{0b} + \Omega_{0\text{nom}})t + \phi_{2b}(t)] \\
& + \frac{A_3(t)}{2}\sin[(3\Omega_{0b} + \Omega_{0\text{nom}})t + \phi_{3b}(t)] \\
& + \cdots + \frac{A_m}{2}\sin[(m\Omega_{0b} + \Omega_{0\text{nom}})t + \phi_{mb}(t)] \\
& + \cdots + \frac{A_{N_h}}{2}\sin[(N_h\Omega_{0b} + \Omega_{0\text{nom}})t + \phi_{N_hb}(t)] \\
& - \frac{A_1(t)}{2}\sin[(\Omega_{0b} - \Omega_{0\text{nom}})t + \phi_{1b}(t)] \\
& - \frac{A_2(t)}{2}\sin[(2\Omega_{0b} - \Omega_{0\text{nom}})t + \phi_{2b}(t)] \\
& - \frac{A_3(t)}{2}\sin[(3\Omega_{0b} - \Omega_{0\text{nom}})t + \phi_{3b}(t)] \\
& + \cdots - \frac{A_m(t)}{2}\sin[(m\Omega_{0b} - \Omega_{0\text{nom}})t + \phi_{mb}(t)] \\
& + \cdots - \frac{A_{N_h}}{2}\sin[(N_h\Omega_{0b} - \Omega_{0\text{nom}})t + \phi_{N_hb}(t)],
\end{aligned} \tag{41}$$

respectively.

From the above equations, one can see that in the signals $y_{ca}(t)$, $y_{sa}(t)$, $y_{cb}(t)$ and $y_{sb}(t)$, around the frequencies 0, $\Omega_{0\text{nom}}$, $2\Omega_{0\text{nom}}$, $3\Omega_{0\text{nom}}, \ldots$, $m\Omega_{0\text{nom}}, \ldots$, one has the frequency components shown in Table 1.

Based on Table 1 and considering that $\Omega_{0a} < \Omega_0 < \Omega_b$, one has

$$\begin{aligned}
& (m+1)\Omega_{0a} - \Omega_{0\text{nom}} < (m-1)\Omega_{0a} + \Omega_{0\text{nom}} \\
& < (m-1)\Omega_{0b} + \Omega_{0\text{nom}} < (m+1)\Omega_{0b} - \Omega_{0\text{nom}},
\end{aligned} \tag{42}$$

Thus, the range of variation of the m-harmonic component is

$$\begin{aligned}
\Delta\Omega_m &= [(m+1)\Omega_{0b} - \Omega_{0\text{nom}}] - [(m+1)\Omega_{0a} - \Omega_{0\text{nom}}] \\
&= (m+1)(\Omega_{0b} - \Omega_{0a}),
\end{aligned} \tag{43}$$

It is noted in (18) that $\Delta\Omega_m$ increases with the increase of the harmonic order m. This is illustrated in Fig. 3 for digital frequencies.

Table 1 Frequency components around the frequencies 0, $\Omega_{0\,\text{nom}}$, $2\Omega_{0\,\text{nom}}$, $3\Omega_{0\,\text{nom}}$, …, $m\Omega_{0\,\text{nom}}$, … for the signals $y_{ca}(t)$, $y_{sa}(t)$, $y_{cb}(t)$ and $y_{sb}(t)$

Central frequency	Frequency components of $y_{ca}(t)$ and $y_{sa}(t)$		Frequency components of $y_{cb}(t)$ and $y_{sb}(t)$	
0	$\Omega_{0\text{nom}} - \Omega_{0a}$	–	$\Omega_{0\text{nom}} - \Omega_{0b}$	–
$\Omega_{0\text{nom}}$	$2\Omega_{0a} - \Omega_{0\text{nom}}$	–	$2\Omega_{0b} - \Omega_{0\text{nom}}$	–
$2\Omega_{0\text{nom}}$	$3\Omega_{0a} - \Omega_{0\text{nom}}$	$\Omega_{0a} + \Omega_{0\text{nom}}$	$3\Omega_{0b} - \Omega_{0\text{nom}}$	$\Omega_{0b} + \Omega_{0\text{nom}}$
$3\Omega_{0\text{nom}}$	$4\Omega_{0a} - \Omega_{0\text{nom}}$	$2\Omega_{0a} + \Omega_{0\text{nom}}$	$4\Omega_{0b} - \Omega_{0\text{nom}}$	$2\Omega_{0b} + \Omega_{0\text{nom}}$
$m\Omega_{0\text{nom}}$	$(m+1)\Omega_{0a} - \Omega_{0\text{nom}}$	$(m-1)\Omega_{0a} - \Omega_{0\text{nom}}$	$(m+1)\Omega_{0b} - \Omega_{0\text{nom}}$	$(m-1)\Omega_{0b} - \Omega_{0\text{nom}}$
$(N_h-1)\Omega_{0\text{nom}}$	$N_h\Omega_{0a} + \Omega_{0\text{nom}}$	$(N_h-2)\Omega_{0a} + \Omega_{0\text{nom}}$	$N_h\Omega_{0b} - \Omega_{0\text{nom}}$	$(N_h-2)\Omega_{0b} + \Omega_{0\text{nom}}$
$N_h\Omega_{0\text{nom}}$	–	$(N_h-1)\Omega_{0a} + \Omega_{0\text{nom}}$	–	$(N_h-1)\Omega_{0b} + \Omega_{0\text{nom}}$
$(N_h+1)\Omega_{0\text{nom}}$	–	$N_h\Omega_{0a} + \Omega_{0\text{nom}}$	–	$(N_h\Omega_{0b}) + \Omega_{0\text{nom}}$

doi: 10.1049/iet-gtd.2010.0565